Journal of Constructional Steel Research 115 (2015) 252–262

Contents lists available at ScienceDirect

Journal of Constructional Steel Research

Analytical buckling of slender circular concrete-filled steel tubular columns with compliant interfaces

S. Schnabl [a,*], G. Jelenić [b], I. Planinc [a]

[a] University of Ljubljana, Faculty of Civil and Geodetic Engineering, Jamova cesta 2, 1001 Ljubljana, Slovenia
[b] University of Rijeka, Faculty of Civil Engineering, Radmile Matejčić 3, 51000 Rijeka, Croatia

ARTICLE INFO

Article history:
Received 23 April 2015
Received in revised form 20 July 2015
Accepted 27 August 2015
Available online xxxx

Keywords:
Buckling
Concrete-filled
Steel
Tube
CFST
Compliant

ABSTRACT

This paper presents an efficient mathematical model for studying the global buckling behavior of concrete-filled steel tubular (CFST) columns with compliant interfaces. The present mathematical model is used to evaluate exact critical buckling loads and modes of CFST columns for the first time. The results prove that the presence of finite interface compliance may significantly reduce the critical buckling load of CFST columns. A good agreement between analytical and experimental buckling loads of circular CFST columns is obtained if at least one among longitudinal and radial interfacial stiffnesses is high. The design methods compared in the paper give conservative results in comparison with the experimental results and analytical results for almost perfectly bonded layers. The parametric study reveals that critical buckling loads of CFST columns are very much affected by the diameter-to-depth ratio and concrete elastic modulus. Moreover, a material nonlinearity has a pronounced effect for short CFST columns, and a negligible effect for slender ones.

1. Introduction

Concrete-filled steel tubular (CFST) columns have been used increasingly in many structural applications including columns supporting platforms of offshore structures and wind turbines, roofs of storage tanks, bridge piers, piles, and columns in seismic zones and high-rise buildings. CFST columns have superior stiffness, strength, ductility, seismic and fire resistance, and deformation characteristics as compared to hollow steel tubes and reinforced concrete columns. Additionally, CFST columns are economical and permit rapid construction because the steel tube serves as a permanent formwork and lateral confinement to the concrete fill, located at the most efficient position. On the other hand, the concrete infill increases local and global buckling resistance of CFST columns and forces the steel tube to buckle outwards rather than inwards. Moreover, with the development of self-compacting, high-strength, ultra-high-strength, lightweight, recycled aggregate concretes, and high-strength and stainless steels, the CFST construction has become even more popular in the construction industry world-wide.

Accordingly, a great deal of experimental [1–12], numerical [13–24], and analytical [25–29] work has been carried out recently to investigate the behavior of CFST columns under various loading conditions. A state of the art knowledge on steel–concrete composite columns including experimental and analytical studies has been reported by Shanmugam and Lakshimi [30] to highlight the significant research in this area until 1999. Similarly, Han et al. [31], have reviewed the development and advanced applications of the family of concrete-filled steel tubular structures till today.

In addition, it is well known that CFST columns can sustain large axial loads. Shorter CFST columns may fail by crushing of the concrete core accompanied by local buckling and yielding of the steel tube while slender CFST columns may fail by local or overall buckling. Despite numerous publications on CFST columns covered in literature, most of research work is focused on short CFST columns. Much less literature is available on global buckling behavior of slender CFST columns, and only a few papers have dealt with this subject, see e.g. [21, 32–35]. To date, however, only Han [36] has experimentally investigated circular CFST columns with very high slenderness ratios.

From the above-mentioned research work done on CFST columns, most of the approaches seem to be based on a simple prediction of fully bonded interface between the concrete core and steel tube. However, there is a major difficulty in the design of CFST columns, which is the imperfect interface compliance between the concrete and steel tube during the initial elastic stage with high axial loads. This happens because steel dilates more than concrete. This imperfect bonding can reduce the confining pressure provided by the steel tube and may reduce the initial stiffness and elastic strength of CFST columns considerably. This situation can be even worse for high-strength CFST columns [37]. Nevertheless, research works on composite action in CFST columns are very limited in open literature. Over the years, only a few researchers have studied numerically and experimentally CFST columns with

* Corresponding author.
E-mail address: simon.schnabl@fgg.uni-lj.si (S. Schnabl).

http://dx.doi.org/10.1016/j.jcsr.2015.08.035
0143-974X/

special emphasis on the composite action between the concrete core and the steel tube, see e.g. [28,37–41]. In all these studies it has been found that composite action in CFST columns is still not well understood and remains as a subject of future research.

It is interesting to note that as far as the authors' knowledge is concerned it seems that there is no analytical work in open literature for analyzing buckling problems of circular CFST slender columns with partial interaction between the constituents.

Consequently, the main objective of this study is to formulate an analytically tractable mathematical model for analyzing the buckling behavior of CFST composite columns with compliant interfaces for the first time. For this purpose, the mechanics of layered column theories similar to that recently developed by the authors [42–48] is taken as a theoretical basis in the derivation of the mathematical model for the analytical buckling analysis of CFST composite columns with compliant interfaces.

In the first numerical example, the analytical results for critical buckling loads of circular CFST columns with compliant interfaces are compared with the experimental buckling loads obtained by Han [36]. In the second numerical example, the analytical results are compared to the results proposed by different design standards. Finally, in the third numerical example, a parametric study is undertaken to investigate the effect of interfacial compliance, diameter-to-depth ratio, column slenderness, concrete elastic modulus, and material nonlinearity of concrete and steel on buckling loads and modes of circular CFST composite columns with interfacial compliance.

2. Problem formulation and governing equations

Consider an initially straight, planar, CFST circular column as shown in Fig. 1. The CFST column has an undeformed length L and is in general, made from concrete core, c, and a steel tube, s, joined by an interface of negligible thickness and finite stiffness in normal and tangential directions. D and t denote the outer diameter and the wall thickness of the steel tube, respectively. The CFST circular column is placed in the (X,Z) plane of a spatial Cartesian coordinate system with coordinates (X,Y,Z) and unit base vectors $\boldsymbol{E}_X$, $\boldsymbol{E}_Y$ and $\boldsymbol{E}_Z = \boldsymbol{E}_X \times \boldsymbol{E}_Y$. The undeformed reference axis of the CFST circular column is common to both layers. It is parameterized by the undeformed arc-length x. Local coordinate system (x, y, z) is assumed to coincide initially with spatial coordinates, and then follows the deformation of the column. Thus, $x^c \equiv x^s \equiv x \equiv X$, $y^c \equiv y^s \equiv y \equiv Y$, and $z^c \equiv z^s \equiv z \equiv Z$ in the undeformed configuration. For more details on the topic of layered composites, an interested reader is referred to, e.g. [43,44]. The CFST circular column is subjected to a conservative compressive load, P, which acts along the neutral axis of the CFST circular column in such a way that homogeneous stress–strain state of the column in its primary configuration is achieved.

2.1. Governing equations

Additional to the aforementioned assumptions, the formulation of governing equations of the CFST circular column uses the following assumptions: (1) the material is linear or nonlinear elastic; (2) the planar

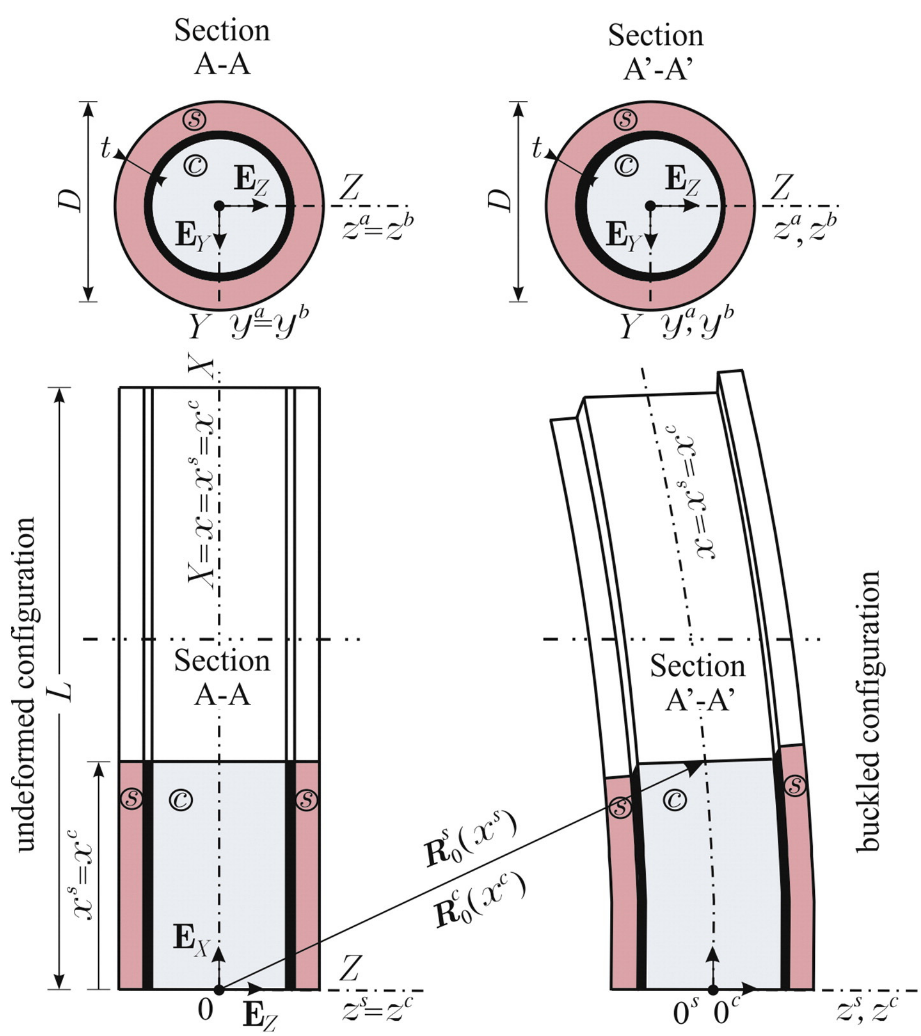

Fig. 1. Undeformed and buckled configuration of CFST circular column.

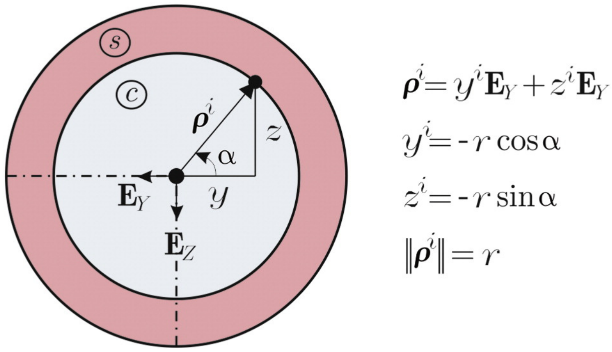

Fig. 2. A cross section of a CFST circular column.

Reissner beam theory [49] is used for each layer; (3) the shear deformations are not taken into account; (4) the layers can slip over each other, and radial separation or uplift between them is possible; (5) the layers are continuously connected and slip and uplift moduli of the connection are constant; (6) the shapes of the layers' cross-sections are symmetrical with respect to the plane of deformation and remain unchanged in the form and size during deformation; and (7) the interlayer slip and uplift are small.

In further expressions, a compact notation $(\bullet)^i$ will be used, where $i=(c,s)$ indicates to which layer the quantity $(\bullet)$ belongs to.

The system of governing equations of the CFST circular column is composed of kinematic, equilibrium, and constitutive equations along with natural and essential boundary conditions for each of the layers. Furthermore, there are also constraining equations that assemble each individual layer into a composite structure.

2.1.1. Kinematic equations

The deformed configurations of the layers reference axes are defined by vector-valued functions (see Fig. 1).

$$\boldsymbol{R}_0^i = X^i\boldsymbol{E}_X + Y^i\boldsymbol{E}_Y + Z^i\boldsymbol{E}_Z = \left(x^i + u^i\right)\boldsymbol{E}_X + y^i\boldsymbol{E}_Y + w^i\boldsymbol{E}_Z. \tag{1}$$

Functions u^i and w^i denote the components of the displacement vector of layer i at the reference axis with respect to the base vectors $\mathbf{E}_X$ and $\mathbf{E}_Z$. The geometrical components u^i and w^i of the vector-valued function $\boldsymbol{R}_0^i$ are further related to the deformation variables by the following equations, see, e.g. [49]:

$$\begin{aligned}
&1 + u^{i'} - \left(1+\varepsilon^i\right)\cos\varphi^i = 0,\\
&w^{i'} + \left(1+\varepsilon^i\right)\sin\varphi^i = 0,\\
&\varphi^{i'} - \kappa^i = 0,
\end{aligned} \tag{2}$$

where the prime (') denotes the derivative with respect to material coordinate x, ε^i is the extensional strain, κ^i is the pseudocurvature, while φ^i is the rotation of the layer's reference axis.

2.1.2. Equilibrium equations

The CFST circular column is subjected longitudinally to a compressive force P at the free end. In addition, each layer of the CFST circular column is subjected to interlayer contact tractions, measured per unit of layer's undeformed length, which are defined by.

$$\boldsymbol{p}^i = p_X^i\boldsymbol{E}_X + p_Z^i\boldsymbol{E}_Z, \tag{3}$$

$$\boldsymbol{m}^i = m_Y^i\boldsymbol{E}_Y. \tag{4}$$

Hence, the equilibrium equations of an individual layer are, see e.g. [44,49]:

$$\begin{aligned}
&R_X^{i'} + p_X^i = 0,\\
&R_Z^{i'} + p_Z^i = 0,\\
&M_Y^{i'} - \left(1+\varepsilon^i\right)\mathcal{Q}^i + m_Y^i = 0.
\end{aligned} \tag{5}$$

where R_X^i, R_Z^i, and M_Y^i represent the generalized equilibrium internal forces of a cross-section of the layer i, with respect to the fixed coordinate basis. The equilibrium axial, $\mathcal{N}^i$, and shear, $\mathcal{Q}^i$, internal forces and bending moments, $\mathcal{M}^i$, of the layers' cross-sections with respect to the rotated local coordinate system can be expressed by.

$$\begin{aligned}
&\mathcal{N}^i = R_X^i\ \cos\ \varphi^i - R_Z^i\ \sin\ \varphi^i,\\
&\mathcal{Q}^i = R_X^i\ \sin\ \varphi^i + R_Z^i\ \cos\ \varphi^i,\\
&\mathcal{M}^i = M_Y^i.
\end{aligned} \tag{6}$$

Table 1
Comparison of analytical and experimental critical buckling loads of CFST P–P column for various K, C, and λ, where $\varepsilon_{cr} \neq 0$, and C and K are in kN/cm^2.

Specimen number	Effective length L [cm]	λ	$N_{cr,e}$ [kN]	C [kN/cm^2]	P_{cr}[kN] $K=10^{-10}$	$K=10^{-2}$	$K=10^{-1}$	$K=1$	$K=10$	$K=10^{10}$
SC154-1	415.8	154	342	10^{-10}	177.712	186.544	240.955	293.753	300.133	300.829
				10^{-5}	190.154	198.154	246.129	293.854	300.134	300.830
SC154-2	415.8	154	292	10^{-3}	295.896	295.931	296.222	297.942	300.220	300.830
SC154-3♣	415.8	154	298	10^{-10}	179.866	188.554	242.275	295.682	302.263	302.983
				10^{-5}	192.105	199.978	247.429	295.785	302.264	302.983
SC154-4♣	415.8	154	280	10^{-3}	297.890	297.926	298.227	300.001	302.687	302.983
SC149-1♣	402.3	149	318	10^{-10}	192.144	200.851	256.099	315.333	322.850	323.672
				10^{-5}	203.669	211.662	261.271	315.444	322.851	323.672
SC149-2♣	402.3	149	320	10^{-3}	317.454	317.501	317.891	320.133	322.947	323.672
SC141-1	380.7	141	350	10^{-10}	212.006	220.886	279.354	348.803	357.908	358.900
				10^{-5}	222.583	230.882	284.535	348.924	357.909	358.900
SC141-2	380.7	141	370	10^{-3}	350.485	350.556	351.142	354.347	358.014	358.900
SC130-1	351.0	130	400	10^{-10}	249.420	258.338	320.144	408.252	420.885	422.25
				10^{-5}	258.493	266.992	325.182	408.395	420.887	422.259
SC130-2	351.0	130	390	10^{-3}	408.493	408.629	409.741	415.378	421.012	422.259
SC130-3♣	351.0	130	440	10^{-10}	252.443	261.215	322.136	410.841	423.862	425.282
				10^{-5}	261.368	269.729	327.126	410.988	423.864	425.282
				10^{-3}	411.089	411.229	412.372	418.177	423.994	425.282

♣ $E^c = 2840$ kN/cm^2.

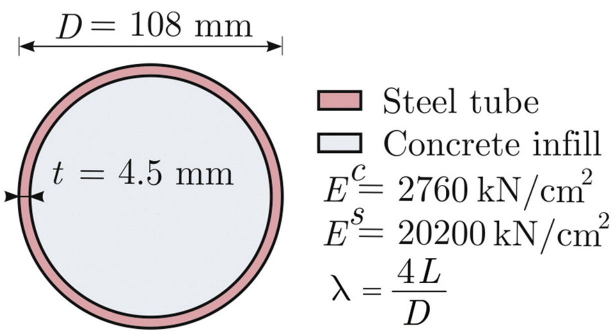

Fig. 3. Geometric and material properties of tested CFST columns.

2.1.3. Boundary conditions

Kinematic (2) and equilibrium (5) equations constitute a set of 12 first order linear differential equations with constant coefficients for 12 unknown functions: u^i, w^i, φ^i, R^i_X, R^i_Z, and M^i_Y. The associated natural and essential boundary conditions are:

$$x^i = 0: \qquad \begin{array}{lll} S^i_1 + R^i_X(0) = 0 & \text{or} & u^i(0) = u^i_1, \\ S^i_2 + R^i_Z(0) = 0 & \text{or} & w^i(0) = u^i_2, \\ S^i_3 + M^i_Y(0) = 0 & \text{or} & \varphi^i(0) = u^i_3, \end{array} \tag{7}$$

$$x^i = L: \qquad \begin{array}{lll} S^i_4 - R^i_X(L) = 0 & \text{or} & u^i(L) = u^i_4, \\ S^i_5 - R^i_Z(L) = 0 & \text{or} & w^i(L) = u^i_5, \\ S^i_6 - M^i_Y(L) = 0 & \text{or} & \varphi^i(L) = u^i_6, \end{array} \tag{8}$$

where u^i_k and $S^i_k (k = 1,2,\ldots,6)$ mark the given values of the generalized boundary displacements and their complementary generalized forces at the edges of layers, i.e. $x^i = 0$ and $x^i = L$, respectively.

2.1.4. Constitutive equations

The constitutive equations of a linear elastic CFST circular column are due to the symmetry of the cross section of the individual layer as follows.

$$\begin{aligned} &\mathcal{N}^i - \mathcal{N}^i_C\left(x^i, \varepsilon^i\right) = \mathcal{N}^i - C^i_{11}\,\varepsilon^i = 0, \\ &\mathcal{M}^i - \mathcal{M}^i_C\left(x^i, \kappa^i\right) = \mathcal{M}^i - C^i_{22}\,\kappa^i = 0, \end{aligned} \tag{9}$$

where $\mathcal{N}^i_C$ and $\mathcal{M}^i_C$ are the constitutive cross-sectional forces dependent only on the deformation variables ε^i and κ^i. Material and geometric constants are marked by C^i_{11} and C^i_{22}; where $C^i_{11} = E^i A^i$, and A^i and E^i denote the cross-sectional area and the Young's modulus of the layer i, respectively; $C^i_{22} = E^i I^i$, where I^i denotes the moment of inertia of the layer i with respect to the reference axis of the CFST circular column.

2.1.5. Constraining equations and interface constitutive model

In the CFST circular column a layer s is constrained to follow the deformation of a layer c and vice versa. This means that the displacements of initially coincident particles in the contact are constrained to each other. This kinematic-constraint relation can be expressed if positions of the observed particles in the deformed configuration are defined as.

$$\boldsymbol{R}^i = X^i \boldsymbol{E}_X + Y^i \boldsymbol{E}_Y + Z^i \boldsymbol{E}_Z, \tag{10}$$

where the spatial Cartesian coordinates X^i, Y^i, and Z^i are dependent on the generalized displacements u^i, w^i, and φ^i as.

$$X^i = x + u^i + z\ \sin\ \varphi^i, \tag{11}$$

$$Y^i = y, \tag{12}$$

$$Z^i = w^i + z\ \cos\ \varphi^i. \tag{13}$$

Thus, the displacement vector between the two initially coincident particles that belong to layer c and s, respectively, is given by.

$$[[\boldsymbol{R}]] = \boldsymbol{R}^c - \boldsymbol{R}^s = \Delta_U \boldsymbol{E}_X + \Delta_W \boldsymbol{E}_Z, \tag{14}$$

or, written in component form as

$$\Delta_U(x, \alpha) = u^c - u^s - r\ \sin\ \alpha(\sin\ \varphi^c - \sin\ \varphi^s), \tag{15}$$

$$\Delta_W(x, \alpha) = w^c - w^s - r\ \sin\ \alpha(\cos\ \varphi^c - \cos\ \varphi^s), \tag{16}$$

where Δ_U and Δ_W mark the interlayer slip and uplift between the observed particles expressed with respect to the unit base vectors $\boldsymbol{E}_X$ and $\boldsymbol{E}_Z$ of a spatial Cartesian coordinate system, and r and α are the polar coordinates of the observed particle in the contact, see Fig. 2.

As a result of the kinematic–constraint relation Eq. (14), interlayer contact tractions evolve. Their magnitudes are dependent on the type of the interface connection. In general, a non-linear interface is modeled using simultaneous sliding and uplifting. Thus, the contact or interlayer tractions.

$$\boldsymbol{p}^{i*} = p^{i*}_X \boldsymbol{E}_X + p^{i*}_Z \boldsymbol{E}_Z, \tag{17}$$

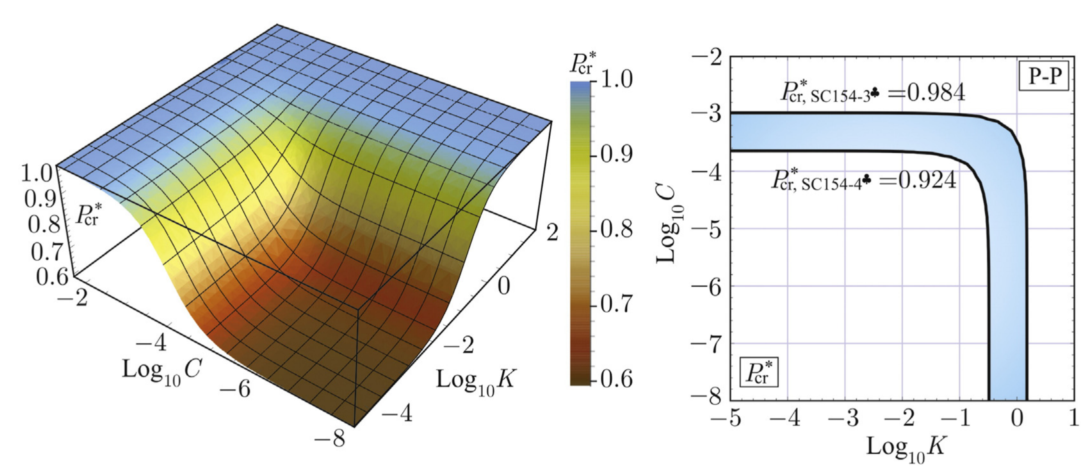

Fig. 4. Comparison of analytical and experimental critical buckling loads of CFST P-P column for various K, C, where $\varepsilon_{cr} = 0$, and C and K are in $\mathrm{kN/cm^2}$. Contours of normalized buckling loads equivalent to the experimental results for specimens SC154-3♣ and SC154-4♣.

are dependent on both Δ_U and Δ_W, see, e.g. [50,51]

$$p_X^{c*}(x,\alpha) = -p_X^{s*}(x,\alpha) = \mathscr{F}^*(\Delta_U,\Delta_W), \tag{18}$$

$$p_Z^{c*}(x,\alpha) = -p_Z^{s*}(x,\alpha) = \mathcal{G}^*(\Delta_U,\Delta_W), \tag{19}$$

where the functions $\mathscr{F}^*$ and $\mathcal{G}^*$ are determined experimentally. Nevertheless, in most civil engineering applications, the interface constitutive laws (18)–(19) can be decoupled. Hence, statically equivalent contact tractions per unit of the reference axis of the CFST circular column are determined by.

$$p_X^i(x) = \int_{C_x^i} p_X^{i*}\mathrm{d}C_x^i = \int_0^{2\pi} \mathscr{F}(\Delta_U)r\mathrm{d}\alpha, \tag{20}$$

$$p_Z^i(x) = \int_{C_x^i} p_Z^{i*}\mathrm{d}C_x^i = \int_0^{2\pi} \mathcal{G}(\Delta_W r\mathrm{d}\alpha), \tag{21}$$

$$\begin{aligned} m_Y^i(x) &= \int_{C_x^i} \rho^i \times \left(p_X^{i*}, 0, p_Z^{i*}\right)\mathrm{d}C_x^i \\ &= \int_0^{2\pi} (0, -r\ \cos\ \alpha, -r\ \sin\ \alpha) \times (\mathscr{F}(\Delta_U), 0, \mathcal{G}(\Delta_W))r\,\mathrm{d}\alpha, \end{aligned} \tag{22}$$

where C_x^i is the contour of the cross-section of layer i, $\mathrm{d}C_x^i$ is its differential, and $\boldsymbol{\rho}^i$. is the cross-sectional vector-valued position function of the observed particle of the layer i in the contact, see Fig. 2.

2.2. Linearized governing equations

A derivation of a linearized system of governing equations for determination of critical buckling loads of CFST columns is based on the first variation (or *Gateaux differential*, *Gateaux variation*) of the nonlinear system of governing Eqs. (2)–(22) defined here as follows [52].

$$\delta\mathscr{F}(\boldsymbol{x},\delta\boldsymbol{x}) = \lim_{\beta\to 0}\frac{\mathscr{F}(\boldsymbol{x}+\beta\delta\boldsymbol{x})-\mathscr{F}(x)}{\beta} = \frac{\mathrm{d}}{\mathrm{d}\beta}\mathscr{F}(\boldsymbol{x}+\beta\delta\boldsymbol{x})\Big|_{\beta=0}, \tag{23}$$

where $\mathscr{F}$ is the functional, $\boldsymbol{x}$ and $\delta\boldsymbol{x}$ are the generalized displacement field and its increment, respectively, and β is a small scalar parameter. In order to derive linearized equations for a CFST column buckling problem, the linearized equations have to be evaluated at the primary configuration of the CFST column, which is an arbitrary deformed configuration in which the CFST column remains straight. Therefore, the primary configuration is determined as.

$$\begin{aligned}
&\varepsilon^i = -\frac{1}{\sum_i C_{11}^i}P,\\
&\kappa^i = 0,\\
&u^i = u^i(0) - \frac{x}{\sum_i C_{11}^i}P\\
&w^i = 0,\\
&\varphi^i = 0,\\
&\Delta_U = 0,\\
&\Delta_W = 0,\\
&R_X^i = \mathcal{N}^i = -\frac{C_{11}^i}{\sum_i C_{11}^i}P,\\
&R_Z^i = \mathcal{Q}^i = 0,\\
&M_Y^i = \mathscr{M}^i = 0,\\
&p_X^i = 0,\\
&p_Z^i = 0,\\
&m_Y^i = 0.
\end{aligned} \tag{24}$$

The linearized stability equations of the CFST composite column, when written at the primary configuration (24), are:

$$\begin{aligned}
&\delta u^{i'} - \delta\varepsilon^i = 0,\\
&\delta w^{i'} + (1+\varepsilon)\delta\varphi^i = 0,\\
&\delta\varphi^{i'} - \delta\kappa^i = 0,\\
&\delta R_X^{c'} - \delta p_X = 0,\\
&\delta R_X^{s'} + \delta p_X = 0,\\
&\delta R_Z^{c'} - \delta p_Z = 0,\\
&\delta R_Z^{s'} + \delta p_Z = 0,\\
&\delta M_Y^{c'} + R_X^c\delta w^{c'} - (1+\varepsilon)\delta R_Z^c - \delta m_Y = 0,\\
&\delta M_Y^{s'} + R_X^s\delta w^{s'} - (1+\varepsilon)\delta R_Z^s + \delta m_Y = 0,\\
&\delta R_X^i - C_{11}^i\delta\varepsilon^i = 0,\\
&\delta M_Y^i - C_{22}^i\delta\kappa^i = 0,\\
&\delta\Delta_U = \delta u^c - \delta u^s - r\sin\alpha(\delta\varphi^c - \delta\varphi^s),\\
&\delta\Delta_W = \delta w^c - \delta w^s,
\end{aligned} \tag{25}$$

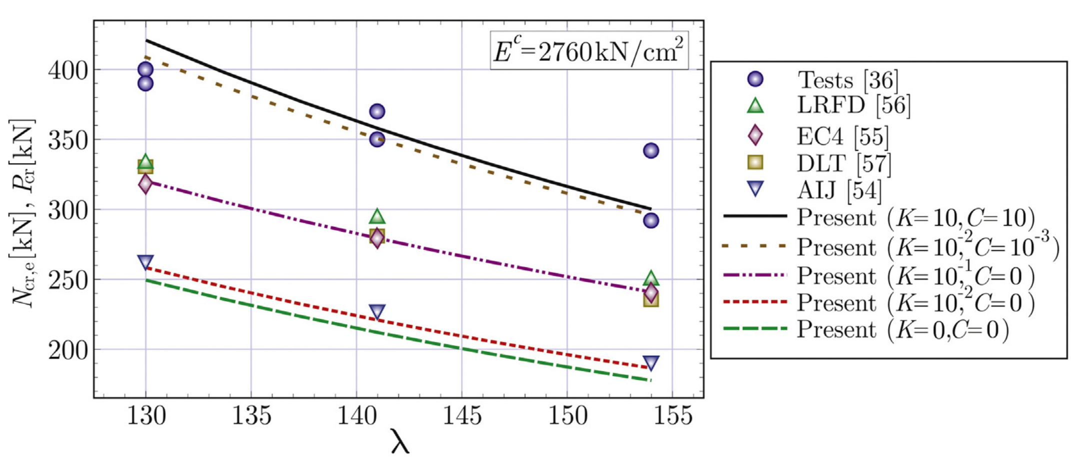

Fig. 5. Comparison between present critical buckling loads and test and code results versus various slenderness ratios, λ, and different contact stiffnesses, C and K, for E^c = 2760 kN/cm^2.

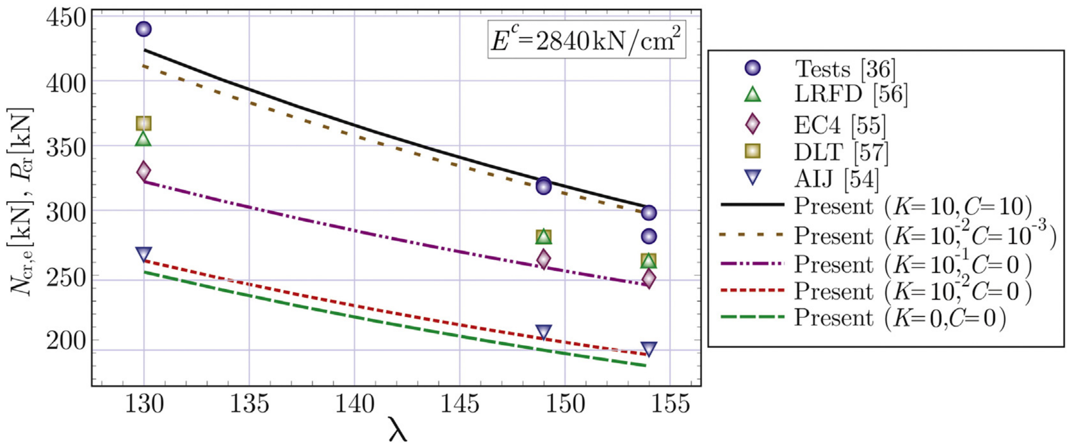

Fig. 6. Comparison between present critical buckling loads and test and code results versus various slenderness ratios, λ, and different contact stiffnesses, C and K, for $E^c = 2840$ kN/cm^2.

where.

$$\begin{aligned}
&\varepsilon = \varepsilon^i = \frac{1}{\sum_i C_{11}^i} P, \\
&\delta p_X = \delta p_X^c = \delta p_X^s = \int_0^{2\pi} K \delta\Delta_U r \mathrm{d}\alpha = 2\pi r K(\delta u^c - \delta u^s), \\
&\delta p_Z = \delta p_Z^c = \delta p_Z^s = \int_0^{2\pi} C \delta\Delta_W r \mathrm{d}\alpha = 2\pi r C(\delta w^c - \delta w^s), \\
&\delta m_Y = \delta m_Y^c = \delta m_Y^s = \int_0^{2\pi} (0, -r\cos\alpha, -r\sin\alpha)\,, \\
&\qquad \times (K\delta\Delta_U, 0, C\delta\Delta_W) r \mathrm{d}\alpha = \pi r^3 K(\delta\varphi^c - \delta\varphi^s)
\end{aligned} \tag{26}$$

and K and C are the longitudinal and radial stiffness of the contact. The system (25) is a system of 18 linear algebraic-differential equations of the first order with constant coefficients for 18 unknown functions $\delta\varepsilon^i$, $\delta\kappa^i$, δu^i, δw^i, $\delta\varphi^i$, δR_X^i, δR_Z^i, δM_Y^i, $\delta\Delta_U$, and $\delta\Delta_W$ along with the corresponding natural and essential boundary conditions:

$$x = 0: \quad \begin{aligned}
&S_1^i + \delta R_X^i(0) = 0 \quad \text{or} \quad \delta u^i(0) = u_1^i, \\
&S_2^i + \delta R_Z^i(0) = 0 \quad \text{or} \quad \delta w^i(0) = u_2^i, \\
&S_3^i + \delta M_Y^i(0) = 0 \quad \text{or} \quad \delta\varphi^i(0) = u_3^i,
\end{aligned} \tag{27}$$

$$x = L: \quad \begin{aligned}
&S_4^i + \delta R_X^i(L) = 0 \quad \text{or} \quad \delta u^i(L) = u_4^i, \\
&S_5^i + \delta R_Z^i(L) = 0 \quad \text{or} \quad \delta w^i(L) = u_5^i, \\
&S_6^i + \delta M_Y^i(L) = 0 \quad \text{or} \quad \delta\varphi^i(L) = u_6^i,
\end{aligned} \tag{28}$$

where u_k^i and $S_k^i (k = 1,2,\ldots,6)$ mark the given values of the generalized boundary displacements and their complementary generalized forces at the edges of layers, i.e. $x = 0$ and $x = L$, respectively.

2.3. Exact solution of the buckling problem

The system of linear algebraic-differential Eq. (25) and the corresponding boundary and continuity conditions (27)–(28) can be written as a homogeneous system of 12 first order linear differential equations as.

$$\boldsymbol{Y}'(x) = \boldsymbol{A}\boldsymbol{Y}(x), \tag{29}$$

and.

$$\boldsymbol{Y}(0) = \boldsymbol{Y}_0, \tag{30}$$

where $\boldsymbol{Y}(x)$. is the vector of unknown functions, $\boldsymbol{Y}(0)$. is the vector of unknown integration constants, and $\boldsymbol{A}$ is the constant

Table 2
Critical buckling loads of circular CFST P–P column for various K and C, where $\varepsilon_{cr} = 0$, $\lambda = 154$, and $E^c = 2840$ kN/cm^2.

P_{cr}[kN]							
C^{**}							
K^{**}	10^{-10}	10^{-7}	10^{-5}	10^{-4}	10^{-3}	10^{-2}	10^{5}
10^{-10}	179.802788$^♠$	179.930873$^♠$	192.041964	255.772185	297.723516	302.302152	302.804855$^⊙$
10^{-5}	179.811750	179.939827	192.050117	255.774758	297.723552	302.302152	302.804855$^⊙$
10^{-4}	179.892379	180.020386	192.123470	255.797905	297.723875	302.302155	302.804855$^⊙$
10^{-3}	180.696203	180.823493	192.854450	256.028334	297.727102	302.302187	302.804855$^⊙$
10^{-2}	188.484417	188.604452	199.908570	258.232043	297.759154	302.302504	302.804855$^⊙$
10^{-1}	242.160490	242.215593	247.314306	273.084338	298.058783	302.305648	302.804855$^⊙$
1	295.511451	295.512505	295.615418	296.433335	299.828050	302.335054	302.804855$^⊙$
10^{1}	302.085640	302.085650	302.086669	302.095798	302.175767	302.509210	302.804855$^⊙$
10^{2}	302.733063	302.733063	302.733074	302.733166	302.734076	302.742046	302.804855$^⊙$
10^{3}	302.797677	302.797677	302.797677	302.797678	302.797688	302.797778	302.804855$^⊙$
10^{4}	302.804137	302.804137	302.804137	302.804137	302.804137	302.804138	302.804855$^⊙$
10^{5}	302.804783	302.804783	302.804783	302.804783	302.804783	302.804783	302.804855$^⊙$
10^{10}	302.804855$^⊙$	302.804855$^⊙$	302.804855$^⊙$	302.804855$^⊙$	302.804855$^⊙$	302.804855$^⊙$	302.804855$^⊙$

** In [kN/cm^2].
♠ $P_{cr} = P_{cr}^{♠}$.
⊙ $P_{cr} = P_{cr}^{⊙}$.

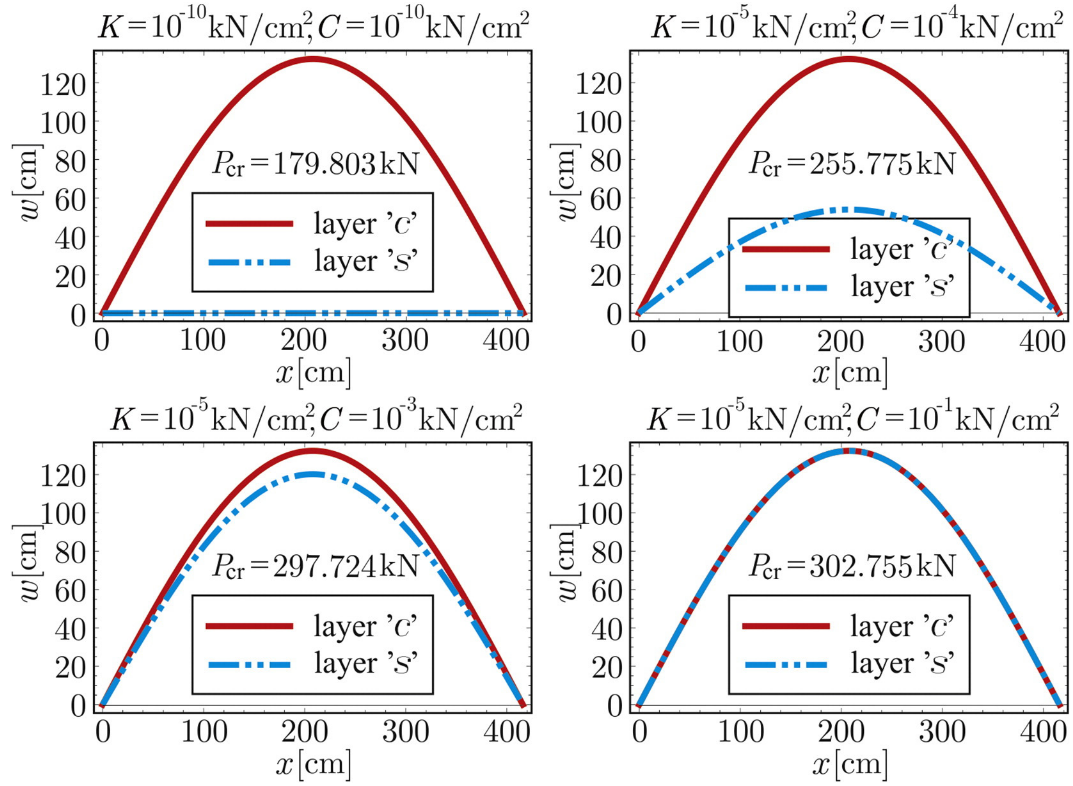

Fig. 7. First buckling modes of layers *c* and *s*, and critical buckling loads of CFST P–P composite column for various values of *K* and *C*.

real 12 × 12 matrix. The exact solution of the problem is given by, see e.g. [53]:

$$\boldsymbol{Y}(x) = \exp^{\boldsymbol{A}x}\boldsymbol{Y}_0. \tag{31}$$

The unknown integration constants which are in this case the initial values of the generalized equilibrium internal forces and components of the displacement vectors, are determined from the boundary conditions (27)–(28). As a result, a system of 12 homogeneous linear algebraic equations for 12 unknown constants is obtained.

$$\boldsymbol{K}\boldsymbol{Y}_0 = 0, \tag{32}$$

where $\boldsymbol{K}$denotes the tangent stiffness matrix. A non-trivial solution of Eq. (32) is obtained from the condition of vanishing determinant of the matrix $\boldsymbol{K}$.

$$\det\boldsymbol{K} = 0. \tag{33}$$

The condition (33) represents a linear eigenvalue problem. Its solution, i.e. the eigenvalues and eigenvectors correspond to the critical buckling loads, P_{cr}, and critical buckling modes of the column. The exact solution for the lowest buckling load, P_{cr}, and corresponding buckling mode can easily be determined but are generally too cumbersome to be presented as closed-form expressions.

3. Numerical examples and discussion

In the first example, the analytical results for critical buckling loads of circular CFST composite column with compliant interfaces are compared with the experimental buckling loads obtained by Han [36]. In the second example, the analytical results are compared to the results proposed by different design standards. Finally, in the third example, a parametric study is undertaken to investigate the effect of interfacial compliance, diameter-to-depth ratio, column slenderness, concrete elastic modulus, and material nonlinearity on the buckling loads and modes of circular CFST composite columns with interfacial compliance.

3.1. Comparison of analytical and experimental results

In order to compare the analytical results of the proposed model with the experimental results in the literature, the critical buckling loads, P_{cr}, of the CFST P–P (pinned–pinned) circular column are calculated and compared to the experimental results, $N_{cr,e}$, obtained by Han [36]. The details of each tested column are listed in Table 1 and shown in Fig. 3. Besides, the exact buckling loads of eleven CFST columns are summarized in Table 1 for various interfacial stiffnesses, *K* and *C*, and column slenderness ratios, λ.

It can be seen from Table 1 that good agreement between analytical and experimental results exists if at least one (longitudinal or radial) interface stiffness is high. In all other cases, the analytical buckling loads are significantly reduced by finite interface compliance. Thus,

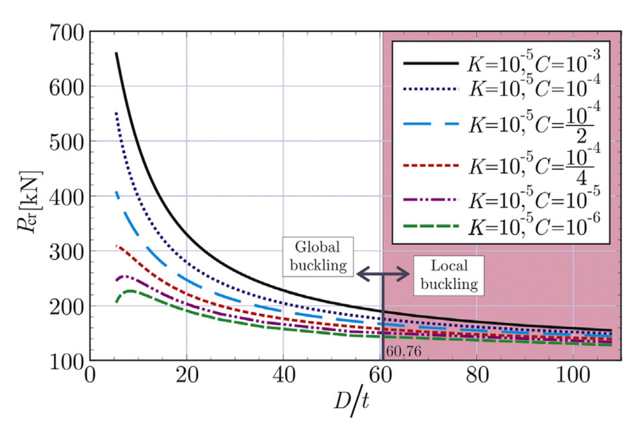

Fig. 8. Effect of diameter-to-thickness ratio on critical buckling loads of circular P–P CFST composite columns for various interfacial stiffnesses *K* and *C*.

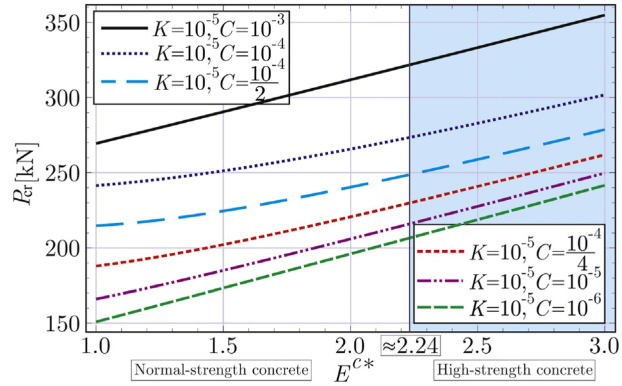

Fig. 9. Effect of concrete elastic modulus, E^c, on critical buckling loads of circular P–P CFST composite columns for various interfacial stiffnesses K and C, where $D/t = 24$ and $\lambda = 154$.

the analytical buckling loads are in the case of almost completely debonded layers up to approximately 60% of those where layers are fully connected to each other, and in the range of 57–64% of experimental results. Note also that some of the experimental results (see, SC154-1, SC141-2, and SC130-3♣) are even higher than those analytical results where full composite action between the steel tube and the concrete core is assumed. The reason for this may lie in the fact that average material properties of concrete core and steel tube were taken in the analytical calculations.

Furthermore, it would be interesting to estimate, what interfacial compliance (C and K) considered in the analytical calculations corresponds to particular experimental results. To this end, the experimental buckling loads of the specimens SC154-3♣ and SC154-4♣ are compared to the analytical results calculated for a wide range of parameters C and K, see Fig. 4. Note that P^*_{cr} is the normalized buckling load of the CFST column defined as $P^*_{cr} = P_{cr}/P_E$, where P_E is the Euler buckling load for the CFST column with perfectly bonded interface between the steel tube and the concrete core. Hence, if the contours for $P^*_{cr,SC154-3^♣} = 0.984$ and $P^*_{cr,SC154-4^♣} = 0.924$ are plotted, see Fig. 4, and estimated as an upper and lower limit, it could be seen that experimental results in this case correspond to the interfacial compliance in the range of either $C \cong [4.36 \cdot 10^{-5}, 10^{-3}]$ kN/cm^2 and $K \le 1.510$ kN/cm^2 or $C \le 10^{-3}$ kN/cm^2 and $K \cong [0.354, 1.510]$ kN/cm^2. From the results in Table 1, it can be seen, that the analytical results for relatively stiff connection ($C \ge 10^{-3}$ kN/cm^2 and $K \ge 1$ kN/cm^2) are within the ± 10% range measured from the mean experimental results. Finally, from the results presented in Table 1 and Fig. 4, it can be concluded that compliant interfaces may lead to a significant reduction of the analytical buckling loads of CFST columns. On the other hand, a comparison reveals that these particular experimental results correspond to the analytical buckling loads of almost perfectly bonded interfaces.

3.2. Comparison of analytical and code results

The proposed analytical buckling loads of CFST columns with compliant interfaces between the concrete core and steel tube are compared to the buckling loads calculated from different design methods such as AIJ [54], Eurocode 4 [55], LRFD [56], and DL/T 5085 [57]. The design results are summarized from Han [36]. It should be emphasized also that the material partial safety factors proposed by all design codes are set to unity when comparing design calculations with analytical and experimental results. A comparison between the proposed analytical buckling loads and test and code results is given in Figs. 5-6 for various slenderness ratios, λ, different contact stiffnesses, C and K, and two different values of concrete elastic modulus, E^c.

It is, however, clear that all the design methods give conservative results in comparison with experimental and analytical results and therefore underestimate the buckling loads of CFST columns considerably. This has already been shown by many researchers, e.g. [7,8,36]. Furthermore, the results shown in Figs. 5-6, indicate, that the buckling loads calculated by Japanese design code [54] are almost equivalent to the analytical results for totally compliant interfaces between the concrete core and steel tube. From both figures it can be seen also that the results of other design codes, namely, American design code [56], Chinese design code [57], and Eurocode 4 [55], correspond between themselves and to the analytical results for intermediately compliant interfaces. As would be expected, an increase of the column slenderness, λ, leads to a significant decrease of the column buckling loads.

3.3. Parametric study

In this section, four illustrative examples are given. The first example is introduced to study the effect of the interface compliance on critical buckling loads and modes of CFST columns. The second and third are devoted to the effect of the diameter-to-thickness ratio, D/t, and concrete elastic modulus, E^c, on critical buckling loads, respectively. The last example pertains to the effect of material nonlinearity on critical buckling loads of CFST columns.

3.3.1. Effect of interface compliance on buckling loads and modes

In what follows, a parametric study is undertaken to investigate the effect of interface compliance on critical buckling loads and modes of CFST columns. For this purpose, a CFST column with the same geometric and material properties as specimens SC154-3♣ and SC154-4♣ is used in the parametric analysis, see Fig. 3 and Table 1. The critical buckling loads

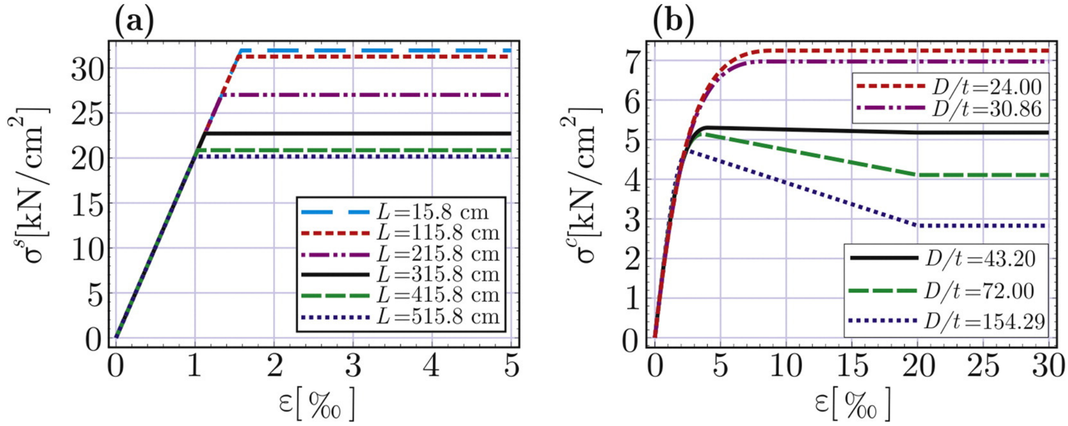

Fig. 10. (a) Idealized bilinear elastic–plastic constitutive laws of compressive steel for $D/t = 24$ and various column lengths; (b) idealized uniaxial stress–strain material laws of confined concrete in circular CFST tubes for $L = 415.8$ cm and various D/t ratios.

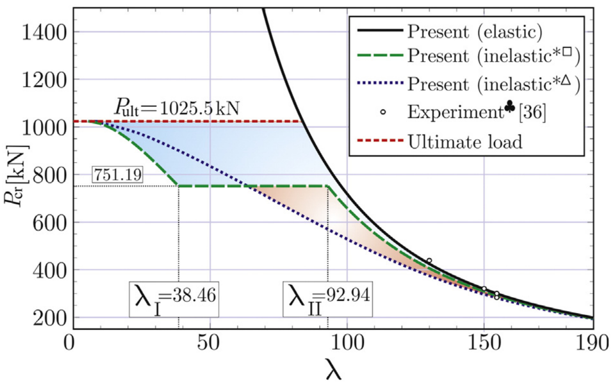

Fig. 11. Elastic and inelastic buckling curves of circular P–P CFST composite columns for various column slenderness, λ and different material laws and $D/t = 24$, where the following notation means: *concrete from [15]; □steel from [13]; △steel from [22]; ♣$E^c = 2840$ kN/cm^2.

are computed by the proposed analytical model for various interlayer stiffnesses K and C. The results are presented in Table 2.

Evidently, the effect of interface compliance, namely the longitudinal and radial interlayer stiffnesses, K and C, on critical buckling loads of CFST columns is significant. It is seen from Table 2 that critical buckling loads can decrease significantly as the longitudinal and radial interlayer stiffnesses, K and C, decrease. However, this effect is insignificant if at least one among stiffnesses is high. Note for example, that in the limiting case when at least one among stiffnesses tends to infinity, the critical buckling load becomes K and C independent. In this case, the critical buckling load of the CFST column corresponds to a total sum of the critical buckling loads of individual layers, namely the buckling load of the concrete core, P^c_{cr}, and the steel tube, P^s_{cr}, respectively,

$$P^{\odot}_{cr} = P^c_{cr} + P^s_{cr} = \frac{\pi^2 (C^c_{22} + C^s_{22})}{(1+\varepsilon)L^2} = \frac{\pi^2 (E^c J^c + E^s J^s)}{(1+\varepsilon)L^2}, \tag{34}$$

and is therefore equivalent to P_E which is the Euler buckling load for the CFST column with perfectly bonded layers. On the contrary, in the limiting case when layers are fully debonded, it may be seen that the critical buckling load of the CFST column under consideration is

$$P^{\clubsuit}_{cr} = P^c_{cr} + P^s + P^s = \frac{\pi^2 C^c_{22}}{(1+\varepsilon)L^2} + C^s_{11}\varepsilon = \frac{\pi^2 E^c J^c}{(1+\varepsilon)L^2} + E^s A^s \varepsilon, \tag{35}$$

where P^s is the axial load carried by the steel tube. This result is expected since the critical buckling load of the concrete core in this particular case is almost as much as 3 times lower than the steel tube. At the end of this example, first buckling modes of the individual layers c and s of the CFST P-P composite column are calculated for various Ks and Cs. The results are plotted in Fig. 7.

It can be seen from Fig. 7 that in case of fully debonded layers, when K and C are almost negligible, only the concrete core buckles, while the steel tube remains straight. However, for all other values of K and C the deformations of the layers become constrained. This effect, however, becomes pronounced for rather rigidly connected layers in either of the two directions. Namely, in that case the first buckling modes of the two layers practically coincide.

3.3.2. Effect of diameter-to-thickness ratio on buckling loads

The effect of the diameter-to-thickness ratio, D/t, where D and t are the outer diameter and the wall thickness of the steel tube, respectively, on critical buckling loads of circular CFST composite columns is studied using the analytical model developed. The effect is studied for the CFST column (i.e., specimen SC154-3♣) whose geometric and material properties are given in Fig. 3 and Table 1. The D/t ratios are considered by changing the thickness of the steel tube walls. Thus, D/t ratio is small when the steel tube thickness is relatively large compared with its diameter, and is, on the other hand, large when the steel tube thickness is relatively small compared with the diameter of the steel tube. The effects of D/t ranging from 5 to 110 on critical buckling loads are shown in Fig. 8 for various interface compliance. As expected, the critical buckling loads increase as the D/t decreases along with the increase of interface compliance. A slightly different trend is observed for small D/t ratios in case of large interface compliance.

It should be noted that the proposed analytical model for buckling analysis of CFST composite columns is suitable only for their global stability analysis. However, the local buckling of steel tubes with high D/t ratios may reduce the strength of thin-walled CFST columns significantly. To avoid the local buckling of circular CFST columns, the local buckling limit for composite columns and composite compression members according to Eurocode 4 [55] is considered. Therefore, local buckling effects may be neglected for D/t ratios smaller than 21150 fy, where f_y is the yield strength of the steel tube in units of N/mm^2. The validity of the results presented in Fig. 8 is thus limited according to Eurocode 4 [55] by D/t ratio smaller than 60.76.

3.3.3. Effect of concrete elastic modulus on buckling loads

The effect of concrete elastic modulus, E^c, on buckling loads of circular CFST slender columns is investigated in Fig. 9. To this end, the buckling loads are calculated for the CFST column with the same geometric and material properties as in the previous examples but for various normalized elastic moduli, $E^{c*} = E^c/E^c_0$, and different interfacial stiffnesses K and C, where $E^c_0 = 1700$ kN/cm^2 is chosen as reference concrete elastic modulus. As anticipated, there is a general trend showing that increasing the concrete elastic modulus increases the critical buckling load of CFST columns in all cases of their interface compliance. Note that for normal-strength concrete, e.g. for concrete of strength class C25/30 according to Eurocode 2 [58], with $E^{c*} = 1.82$ and $K = 10^{-5}$ kN/cm^2, the critical buckling loads are $P_{cr}[C = 10^{-6}] = 188.024$ kN; $P_{cr}[C = 10^{-5}] = 198.461$ kN; $P_{cr}[C = 10^{-4}] = 260.218$ kN; $P_{cr}[C = 10^{-3}] = 304.216$ kN; while, for high-strength concrete, e.g. for concrete of strength class C90/105 [58] with $E^{c*} = 2.59$, the critical buckling loads are $P_{cr}[C = 10^{-6}] = 222.818$ kN; $P_{cr}[C = 10^{-5}] = 231.555$ kN; $P_{cr}[C = 10^{-4}] = 286.138$ kN; $P_{cr}[C = 10^{-3}] = 336.970$ kN. Evidently, the effect of concrete elastic modulus on the critical buckling load is

Table 3
Comparison of elastic and inelastic critical buckling loads of circular P–P CFST composite columns for various column slenderness, λ, and different material laws.

P_{cr}[kN]							
λ	Elastic	Inelastic*,□	$\frac{\text{Inelastic}^{*,\square}}{\text{Elastic}}$	Inelastic*,△	$\frac{\text{Inelastic}^{*,\triangle}}{\text{Elastic}}$	Experiment♣	$\frac{\text{Experiment}^{\clubsuit}}{\text{Elastic}}$
130	425.282	405.598	0.954	374.258	0.880	440	1.035
149	323.672	312.994	0.967	300.076	0.927	318 (320)	0.982 (0.989)
159	302.983	293.794	0.970	283.497	0.936	280 (298)	0.924 (0.983)

* Concrete from [15..
□ steel from [13].
△ steel from [22].
♣ $E^c = 2840$ kN/cm^2.

significant. Thus, comparing a high performance concrete to a normal strength concrete, it is seen that the critical buckling loads can increase up to approximately 80% due to the use of higher strength concrete.

3.3.4. Effect of material nonlinearity on buckling loads

The real behavior of CFST columns is rather different from that described in the previous sections. The solution for elastic buckling has a limited use, since such buckling occurs only for very slender columns. Most columns in practice generally fail by inelastic buckling before reaching the Euler buckling loads. Thus, the proposed analytical model for calculating the elastic buckling loads of CFST columns is here simply extended to account for material nonlinearity in case of stiff connection. Hence, condition (33) along with the longitudinal boundary condition constitutes a system of two non-linear algebraic equations

$$f_1(P_{cr},\varepsilon_{cr}) = \det\boldsymbol{K} = (1+\varepsilon_{cr})P_{cr} - \frac{\pi^2\left(C_{22}^c + C_{22}^s\right)}{L^2} = 0, \tag{36}$$

$$f_2(P_{cr},\varepsilon_{cr}) = \mathcal{N}^c + \mathcal{N}^s + P_{cr} = \sigma^c A^c + \sigma^s A^s + P_{cr} = 0, \tag{37}$$

for the two unknowns, i.e. the critical buckling load, P_{cr}, and the critical axial strain, ε_{cr}, of the CFST composite column, where σ^c and σ^s are the stresses in the concrete core and steel tube, respectively. The system Eqs. (36)–(37) is solved numerically using a Newton–Raphson iterative method.

In order to investigate the effect of material nonlinearity on buckling behavior of inelastic circular CFST columns, numerical calculations are carried out by which the exact critical buckling loads of inelastic circular CFST composite columns are determined from Eqs. (36)–(37) using the tangent modulus method for various stress–strain relations of concrete and steel under compression. Firstly, the critical buckling loads are calculated for a stress–strain relationship of the confined concrete in circular CFST columns suggested by Liang and Fragomeni [15], and a bilinear elastic–plastic constitutive law of the compressive steel proposed by Shams and Saadeghvaziri [13], see Fig. 10. Secondly, the bilinear material law for steel is replaced by the full-range three-stage stress–strain relation for steel presented by Quach et al. [59] and used very recently in case of circular CFST columns by Patel et al. [22].

The critical buckling loads of inelastic circular CFST columns are compared with the corresponding elastic buckling loads and with the experimental results published by Han [36] for various column slenderness ratios, λ, in Fig. 11. Also, critical buckling loads for high slenderness ratios are tabulated in Table 3.

Note that the range of application of the elastic critical buckling loads is limited in this case by the plastic squashing load $P_{ult} = 1025.5$ kN. It is seen from Fig. 11 and Table 3, that the effect of material nonlinearity is pronounced especially for short and medium columns. The difference between the elastic and inelastic buckling loads then decreases significantly as the column becomes more slender. Thus, for high column slenderness ratios the effect of material nonlinearity is negligible and the analytical elastic and inelastic buckling loads almost coincide. For example, the discrepancy of the buckling loads for $\lambda = 154$ is only up to approximately 6%, see Table 3. Similarly, it is evident that the experimental results of circular CFST columns with high slenderness ratios [36] lie practically on the Euler elastic curve.

Moreover, by referring to Fig. 11, it is perhaps of interest to note, that if a bilinear elastic–plastic constitutive law for compressive steel is taken into account, the discontinuity in inelastic buckling curve occurs due to a sudden decrease of column's flexural stiffness at the yielding point of steel, which in this particular case corresponds to approximately $P_{cr} = 751.19$ kN. Thus, corresponding to this load, two discontinuity points exist related to slenderness ratio, namely, $\lambda_1 = 38.46$ and $\lambda_2 = 92.94$.

4. Conclusions

The paper presented a new mathematical model for studying the buckling behavior of circular concrete-filled steel tubular (CFST) slender columns with compliant interfaces. The model is capable of predicting exact critical buckling loads and modes of CFST columns. The effect of interface compliance, and various other parameters, on critical buckling loads of CFST was studied in detail. Based on the results obtained in the present study, the following conclusions can be drawn:

1. The analytical buckling loads of elastic circular CFST columns with compliant interfaces are derived for the first time.
2. A good agreement between analytical and experimental buckling loads of circular CFST composite columns is observed if at least one among longitudinal and radial interfacial stiffnesses is high. In the presence of finite interfacial compliance the critical buckling loads are reduced significantly.
3. The design methods compared in the paper give conservative results in comparison with the experimental results and analytical results of circular CFST columns with almost perfectly bonded layers, and therefore underestimate the buckling loads of CFST considerably.
4. The effect of interface compliance on critical buckling loads and modes of CFST columns is proved to be significant. The critical buckling loads decrease as the interfacial compliance increases. The first buckling modes proved to be constrained if a finite interfacial compliance is present.
5. The parametric study reveales that the critical buckling loads of circular CFST columns are also very much affected by the diameter-to-depth ratio and concrete elastic modulus.
6. The investigation of the influence of material nonlinearity on buckling behavior of inelastic circular CFST columns showes that this effect is pronounced for short columns. On the other hand this effect is negligible for slender columns. In that case, the analytical elastic and inelastic buckling loads are very much similar to the experimental buckling loads.
7. The results can be used as a benchmark solution for a buckling problem of circular CFST columns with compliant interfaces

Acknowledgments

The second author acknowledges the support of the Croatian Science Foundation through the research project No IP-11-2013-1631 (configuration-dependent approximation in non-linear finite-element analysis of structures) as well as the University of Rijeka support for ongoing research No 13.05.1.3.06 (testing of slender spatial beam structures with emphasis on model validation).

References

[1] J. Zeghiche, K. Chaoui, An experimental behaviour of concrete-filled steel tubular columns, J. Constr. Steel Res. 61 (2005) 53–66.
[2] E. Ellobody, B. Young, D. Lam, Behaviour of normal and high strength concrete-filled compact steel tube circular stub columns, J. Constr. Steel Res. 62 (5) (2006) 706–715.
[3] Y.F. Yang, L.H. Han, Experimental behaviour of recycled aggregate concrete filled steel tubular columns, J. Constr. Steel Res. 62 (2006) 1310–1324.
[4] L. Guo, S. Zhang, W.J. Kim, G. Ranzi, Behavior of square hollow steel tubes and steel tubes filled with concrete, Thin-Walled Struct. 45 (12) (2007) 961–973.
[5] D. Lam, L. Gardner, Structural design of stainless steel concrete filled columns, J. Constr. Steel Res. 64 (11) (2008) 1275–1282.
[6] J. Chen, W. Jin, Experimental investigation of thin-walled complex section concrete-filled steel stub columns, Thin-Walled Struct. 48 (2010) 718–724.
[7] B. Uy, Z. Tao, L.H. Han, Behaviour of short and slender concrete-filled stainless steel tubular columns, J. Constr. Steel Res. 67 (2011) 360–378.
[8] M. Dundu, Compressive strength of circular concrete filled steel tube columns, Thin-Walled Struct. 56 (2012) 62–70.
[9] M.H. Lai, H. JCM, Confinement effect of ring-confined concrete-filled-steel-tube columns under uni-axial load, Eng. Struct. 67 (2014) 123–141.
[10] Q.X. Ren, L.H. Han, D. Lam, W. Li, Tests on elliptical concrete filled steel tubular (CFST) beams and columns, J. Constr. Steel Res. 99 (2014) 149–160.

[11] P. Feng, S. Cheng, Y. Bai, L. Ye, Mechanical behavior of concrete-filled square steel tube with FRP-confined concrete core subjected to axial compression, Comput. Struct. 123 (2015) 312–324.
[12] Y. Wang, J. Chen, Y. Geng, Testing and analysis of axially loaded normal-strength recycled aggregate concrete filled steel tubular stub columns, Eng. Struct. 86 (2015) 192–212.
[13] M. Shams, M.A. Saadeghvaziri, Nonlinear response of concrete-filled steel tubular columns under axial loading, J. Constr. Steel Res. 96 (6) (1999) 1009–1017.
[14] H.T. Hu, C.S. Huang, M.H. Wu, Y.M. Wu, Nonlinear analysis of axially loaded concrete-filled tube columns with confinement effect, J. Struct. Eng. ASCE 129 (10) (2003) 1322–1329.
[15] Q.Q. Liang, S. Fragomeni, Nonlinear analysis of circular concrete-filled steel tubular short columns under axial loading, J. Constr. Steel Res. 65 (2009) 2186–2196.
[16] H.R. Valipour, S.J. Foster, Nonlinear analysis and cyclic analysis of concrete-filled steel columns, J. Constr. Steel Res. 66 (2010) 793–802.
[17] K.K. Choi, Y. Xiao, Analytical studies of concrete-filled circular steel tubes under axial compression, J. Struct. Eng. ASCE 136 (5) (2010) 565–573.
[18] Q.Q. Liang, High strength circular concrete-filled steel tubular slender beam-columns, part I: numerical analysis, J. Constr. Steel Res. 67 (2011) 164–171.
[19] Z. Tao, Z.B. Wang, Q. Yu, Finite element modelling of concrete-filled steel stub columns under axial compression, J. Constr. Steel Res. 89 (2013) 121–131.
[20] K. Wang, B. Young, Fire resistance of concrete-filled high strength steel tubular columns, Thin-Walled Struct. 71 (2013) 46–56.
[21] M.F. Hassanein, O.F. Kharoob, Analysis of circular concrete-filled double skin tubular slender columns with external stainless steel tubes, Thin-Walled Struct. 79 (2013) 23–37.
[22] V.I. Patel, Q.Q. Liang, H. MNS, Nonlinear analysis of axially loaded circular concrete-filled stainless steel tubular short columns, J. Constr. Steel Res. 101 (2014) 9–18.
[23] D.J. Zhang, Y.S. Ma, Y. Wang, Compressive behavior of concrete filled steel tubular columns subjected to long-term loading, Thin-Walled Struct. 89 (2015) 205–211.
[24] F. Aslani, B. Uy, Z. Tao, F. Mashiri, Behaviour and design of composite columns incorporating compact high-strength steel plates, J. Constr. Steel Res. 107 (2015) 94–110.
[25] S. Schneider, Axially loaded concrete-filled steel tubes, J. Struct. Eng. ASCE 124 (10) (1998) 1125–1138.
[26] J. Brauns, Analysis of stress state in concrete-filles steel column, J. Constr. Steel Res. 49 (1999) 189–196.
[27] S. KAS, H. Ge, T. Usami, Uniaxial stress–strain relationship of concrete confined by various shaped steel tubes, Eng. Struct. 23 (2001) 1331–1347.
[28] A. Fam, F.S. Qie, S. Rizkalla, Concrete-filled steel tubes subjected to axial compression and lateral cyclic loads, J. Struct. Eng. ASCE 130 (4) (2004) 631–640.
[29] A. Kuranovas, D. Goode, A.K. Kvedaras, S. Zhong, Load-bearing capacity of concrete-filled steel columns, J. Civ. Eng. Manag. 15 (1) (2009) 21–33.
[30] N.E. Shanmugam, B. Lakshmi, State of the art report on steel–concrete composite columns, J. Constr. Steel Res. 57 (2001) 1041–1080.
[31] L.H. Han, W. Li, R. Bjorhovde, Developments and advanced applications of concrete-filled steel tubular (CFST) structures: members, J. Constr. Steel Res. 100 (2014) 211–228.
[32] C.D. Goode, A. Kuranovas, A.K. Kvedaras, Buckling of slender composite concrete-filled steel columns, J. Civ. Eng. Manag. 16 (2) (2010) 230–236.
[33] J.M. Portolés, M.L. Romero, F.C. Filippou, J.L. Bonet, Simulation and design recommendations of eccentrically loaded slender concrete-filled tubular columns, Eng. Struct. 33 (5) (2011) 1576–1593.
[34] M.L. Romero, V. Moliner, A. Espinos, C. Ibañez, A. Hospitaler, Fire behavior of axially loaded slender high strength concrete-filled tubular columns, J. Constr. Steel Res. 67 (12) (2011) 1953–1965.
[35] X.H. Dai, D. Lam, N. Jamaluddin, J. Ye, Numerical analysis of slender elliptical concrete filled columns under axial compression, Thin-Walled Struct. 77 (2014) 26–35.
[36] L.H. Han, Tests on concrete filled steel tabular columns with high slenderness ratio, Adv. Struct. Eng. 3 (4) (2000) 337–344.
[37] F.Y. Liao, L.H. Han, S.H. He, Behavior of CFST short column and beam with initial concrete imperfection: experiments, J. Constr. Steel Res. 67 (12) (2011) 1922–1935.
[38] J.F. Hajjar, P.H. Schiller, A. Molodan, A distributed plasticity model for concrete-filled steel tube beam-columns with interlayer slip, Eng. Struct. 20 (8) (1998) 663–676.
[39] C.W. Roeder, B. Cameron, C.B. Brown, Composite action in concrete filled tubes, J. Struct. Eng. ASCE 125 (5) (1999) 477–484.
[40] O.''.S. MD, R.Q. Bridge, Design of circular thin-walled concrete filled steel tubes, J. Struct. Eng. ASCE 126 (11) (2000) 1295–1303.
[41] C.W. Roeder, D.E. Lehman, E. Bishop, Strength and stiffness of circular concrete-filled tubes, J. Struct. Eng. ASCE 136 (12) (2010) 1545–1553.
[42] S. Schnabl, M. Saje, G. Turk, I. Planinc, Analytical solution of two-layer beam taking into account interlayer slip and shear deformation, J. Struct. Eng. ASCE 133 (6) (2007) 886–894.
[43] A. Kryžanowski, S. Schnabl, G. Turk, I. Planinc, Exact slip-buckling analysis of two-layer composite columns, Int. J. Solids Struct. 46 (2008) 2929–2938.
[44] S. Schnabl, I. Planinc, The influence of boundary conditions and axial deformability on buckling behavior of two-layer composite columns with interlayer slip, Eng. Struct. 32 (10) (2010) 3103–3111.
[45] S. Schnabl, I. Planinc, The effect of transverse shear deformation on the buckling of two-layer composite columns with interlayer slip, Int. J. Nonlinear Mech. 46 (3) (2011) 543–553.
[46] S. Schnabl, I. Planinc, Inelastic buckling of two-layer composite columns with non-linear interface compliance, Int. J. Mech. Sci. 53 (12) (2011) 1077–1083.
[47] S. Schnabl, I. Planinc, Exact buckling loads of two-layer composite reissner's columns with interlayer slip and uplift, Int. J. Solids Struct. 50 (2013) 30–37.
[48] A. Kryžanowski, I. Planinc, S. Schnabl, Slip-buckling analysis of longitudinaly delaminated composite columns, Eng. Struct. 76 (2014) 404–414.
[49] E. Reissner, On one-dimensional finite-strain beam theory: the plane problem, J. Appl. Mech. Phys. ZAMP 23 (1972) 795–804.
[50] K.Y. Volokh, A. Needleman, Buckling of sandwich beams with compliant interfaces, Comput. Struct. 80 (2002) 1329–1335.
[51] G. Alfano, M.A. Crisfield, Finite element interface models for the delamination analysis of laminated composites: mechanical and computational issues, Int. J. Numer. Methods Eng. 50 (2001) 1701–1736.
[52] Hartmann, F. The Mathematical Foundation of Structural Mechanics. Springer-Verlag Berlin and Heidelberg GmbH & Co.K.; 1985.
[53] L. Perko, Differential Equations and Dynamical Systems, 3rd ed. Springer-Verlag, New York, 2001.
[54] AIJ, Recommendations for Design and Construction of Concrete Filled Steel Tubular Structures, Architectural Institute of Japan, 1997 (in Japanese).
[55] EN 1994-1–1: Eurocode 4, Design of Composite steel and Concrete Structures, European Committee for Standardization, Brussels, 1992.
[56] AISC, Load and Resistance Factor Design Specification for Structural Steel Buildings, USA, American Institute of Steel Construction. Chicago, 1994.
[57] DL/T 5085, Chinese Design Code for Steel–Concrete Composite Structures, Chinese Electricity Press, 1999 (in Chinese).
[58] EN 1992-1–1: Eurocode 2, Design of Concrete Structures — Part 1–1: General Rules and Rules for Buildings, European Committee for Standardization, Brussels, 1992.
[59] W.M. Quach, J.G. Teng, K.F. Chung, Three-stage full-range stress–strain model for stainless steel, J. Struct. Eng. ASCE 134 (9) (2008) 1518–1527.